



Optimization of the edge effect of 4340 steel specimen heated by induction process with flux concentrators using finite element axis-symmetric simulation and experimental validation

Mohamed Khalifa¹ · Nouredine Barka¹ · Jean Brousseau¹ · Philippe Bocher²

Received: 29 April 2019 / Accepted: 9 August 2019 / Published online: 27 August 2019
© Springer-Verlag London Ltd., part of Springer Nature 2019

Abstract

This research is performed by 2D axis-symmetric finite element simulation based on the coupling of electromagnetic fields and heat transfer applied on 4340 steel specimen with flux concentrators heated by induction process. The model is built using COMSOL software based on an adequate formulation taking into account the material properties and process parameters. The obtained induced currents and temperature distributions are analyzed versus the geometrical dimensions of the model. The originality of this paper lies in the exploitation of simulation data using classical modeling and the optimization techniques to optimize the hardness profile according to geometrical factors. The proposed method is based on finite element simulations and adequate objective function able to converge to the optimal linear hardness profile. The results demonstrate that the final hardness profile can be quasi-uniform with a narrow flux concentrator gap when the gap between the master part and the inductor is larger. This overall study allows a good exploration of hardness profile linearity under various geometrical dimensions and permits a good comprehension of induction heating with flux concentrator behavior.

Keywords Induction heating · 4340 steel disk · 2D model · High frequency · Flux concentrators · Optimization

1 Introduction

The automotive and aerospace manufacturing industry is always in the face of the challenge of the growing demand for more efficient and higher performance components. In order to improve the mechanical behavior of engineering parts such as gears and crankshaft, basic understanding of failure modes is important. During their service, components are subject to cyclic and heavy loads, and crack initiation is linked essentially with the magnitude and direction of stresses applied to the component. Studies have shown that residual stresses play an important role in the distortion of machined components and have an important impact on the fatigue life and the

endurance of the engineering component [1, 2]. Residual stress arise as a consequence of manufacturing and treatment process of the part, especially in those processes where the internal microstructure of the component undergoes volume expansions due to heat treatments such as welding and surface hardening with rapid cooling [3, 2]. Tensile residual stresses are not beneficial as they increase the likelihood of fatigue failure by promoting crack initiation and growth. Otherwise, compressive residual stresses in the surface layer are very beneficial to counteract crack development and to improve stress corrosion cracking resistance and fatigue behavior [3, 4]. The different processes and methods used in the component manufacturing steps therefore all play an important role in the final distribution of residual stresses [5]. Furthermore, many scientists are trying to develop finite element models (FEM) capable of predicting the residual stresses induced by different manufacturing processes [6, 7, 8, 9]. These models will subsequently minimize the distortion phenomenon while reducing the number of steps and also modify the machining methods without affecting the properties of the components.

In induction hardening, where the surfaces of parts such as gears and disk are heated to high temperature with rapid

✉ Mohamed Khalifa
med.kalifa@live.fr

¹ Département de mathématiques, d'informatique et de génie,
Université du Québec à Rimouski, Rimouski, Québec, Canada

² Département de génie mécanique, École de technologie supérieure,
Montreal, Québec, Canada

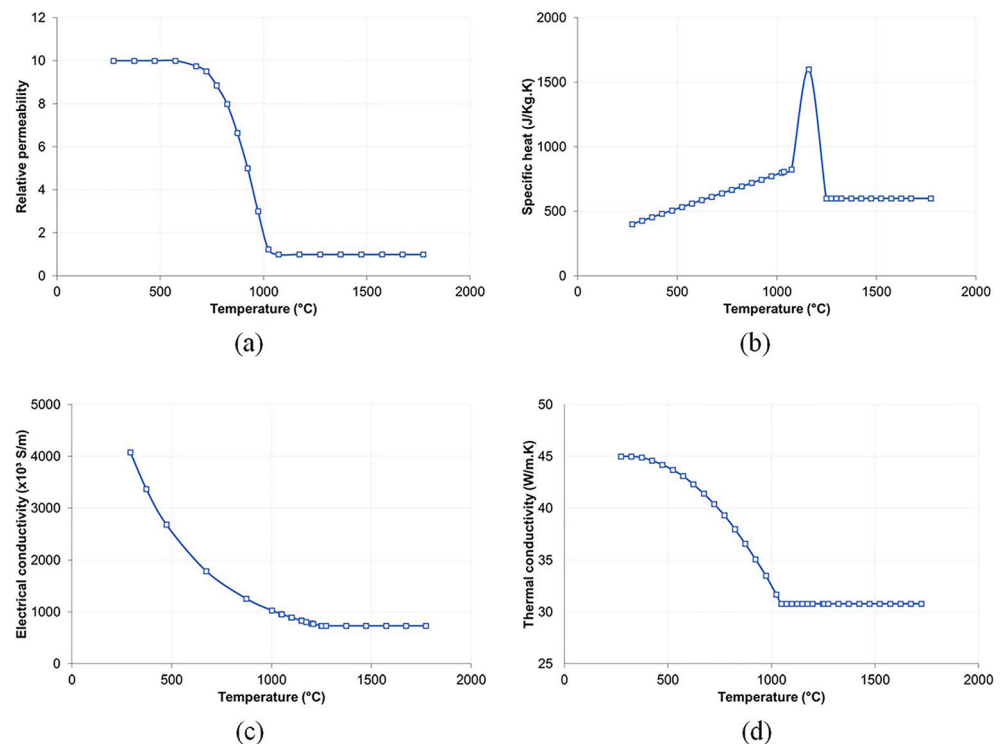
Table 1 Chemical composition of 4340 steel [6]

Element	Ni	Cr	Mn	C	Mo	Si	S	P
Content (%)	1.65–2.00	0.700–0.900	0.600–0.800	0.380–0.430	0.200–0.300	0.150–0.300	0.0400	0.0350

cooling, a compressive residual stress could be conceived by the generation of high temperatures and microstructural and mechanical properties' gradients between the surface layer and the core of the component [10, 11]. Change of austenite to martensite after quenching is accompanied with a hardness and volume increase that is proportional to the carbon percentage contained in the treated material [12]. This thermal expansion due to temperature gradient and phase change produces a beneficial state of compressive residual stress that can be predicted and/or controlled according to several factors involved in the induction heating process, such as the cooling rate [13] and final temperature distribution before quenching ([14, 15]). Furthermore, the fatigue strength is proportional to the thickness of the hardened surface layer and changes depending on the hardness distribution [16]. Indeed, the hardened region is directly related to the microstructure composition which could be interpreted from the final temperature distribution of the heating process. Measuring temperature distribution during the induction heating process is a difficult task to do due to the very quick heating rate of the induction process. Some researchers have developed an experimental method to measure surface temperature profile at the end of induction heating [17]. Therefore, developed FEM models are very useful to

predict accurately the real behavior of the temperature distribution [18], not to mention that experimental designing and testing technologies are always associated with high-cost processes.

It is always advantageous to control temperature distribution at the end of the process. In induction heating of disk and gears with single shot, the non-uniformity of power density distribution is dependent on magnetic field distortion at the surface and near the edge of components, so called the edge effect, which could be predicted and controlled by many factors like system geometry, coil power, frequency, and heating time [19]. Barka et al. [20] introduced a simple and effective approach to reduce the edge effect for gears without affecting coil geometry or process parameters; the technique consists of putting the main gear between two identical gears with some axial gap acting like flux concentrators to the middle part. In this paper, the possibility of optimizing this approach is examined and applied on a disk made of 4340 low carbon steel, using a FEM model coupled with optimization algorithms with experimental validation to generate the optimal geometrical parameters that give the best hardness profile at the end of the process.

Fig. 1 Evolution of electrical, magnetic, and thermal properties versus temperature of the 4340 steel [22]

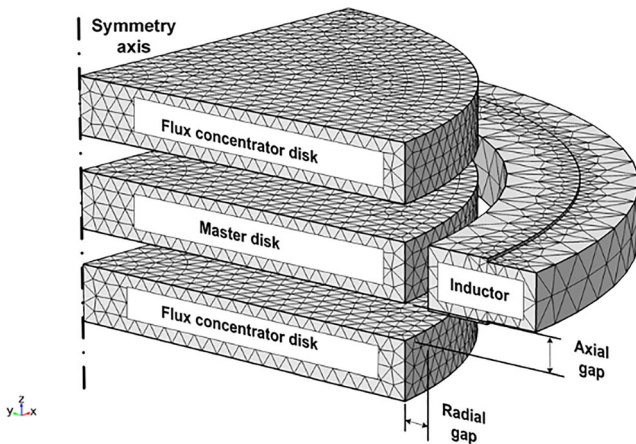


Fig. 2 Schematic presentation of the model geometry

2 Methodology

The chosen model is a finite element model of the coil and the treated parts and is well adapted to complex geometries which guarantee an increased precision of simulated phenomena. The proposed algorithm is based on the coupling between numerical simulations and finite element analysis, with the aim of developing a system capable of automatically generating an optimal configuration. Thus, an iterative procedure is used for dimensioning the different gaps between the process components; it consists of an analysis phase of the geometrical combination intended to be optimized and a minimization phase of the objective function based on the obtained results.

The initial parameters, derived from the experimental data, make it possible to reduce the simulation time and also make it

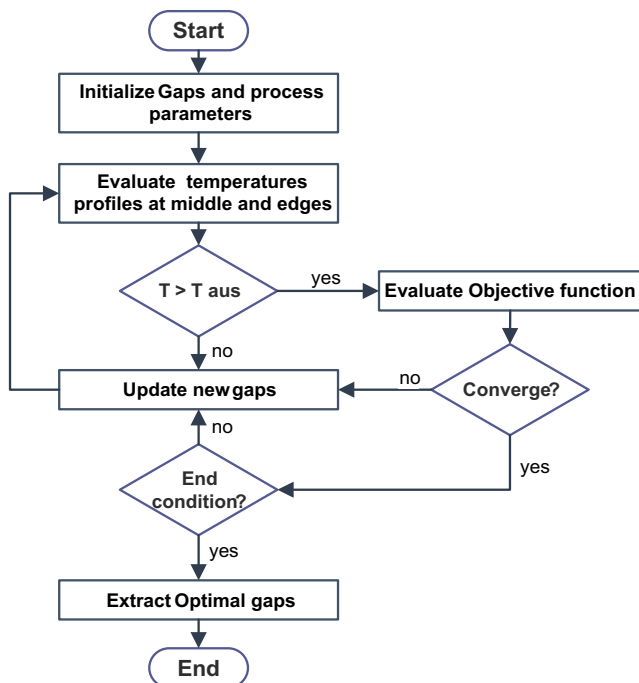


Fig. 3 Flowchart of the optimization procedure

possible to identify the most influential parameters, thus reducing the number of parameters to be optimized before the optimization process, and the computation times are then reduced significantly. However, the desired speed of the optimization study requires a precise analysis of the chosen geometry structure, thus leading to a significant reduction of the exploration of the solution domain. Finally, the proposed algorithm offers a complete solution, resulting in an optimal geometry structure from objective temperature and constraints of the optimization parameters.

3 Parametric study

3.1 Material characterization

The workpiece is a disk made of steel 4340, as used for example in the manufacture of crankshaft crank pins or cranks. The 4340 steel is a material widely used in the automotive and aerospace industry because of its very high hardenability [21]. The 4340 steel is characterized by its robustness, strong toughness, good ductility, and immunity against embrittlement. The thermal and electrical properties of this steel are strongly related to the variation of the temperature (Table 1 and Fig. 1) [21].

4 Geometry

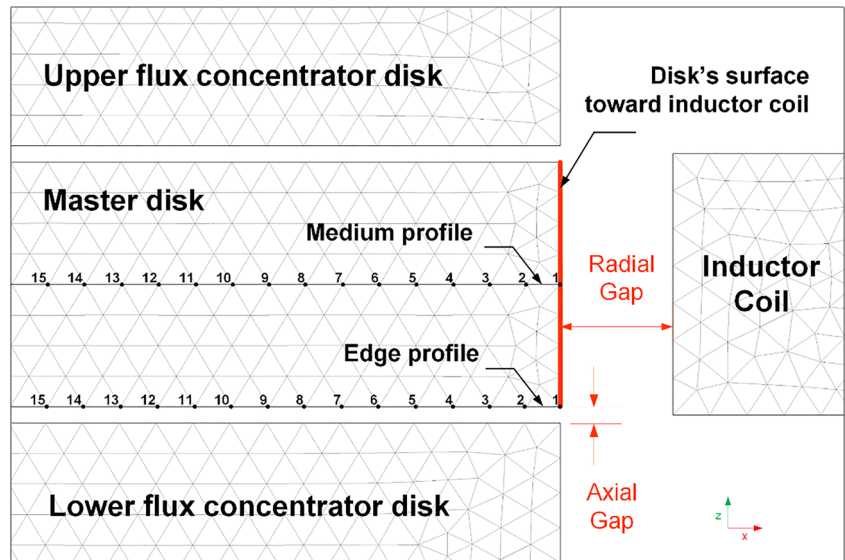
The 4340 steel disk having the properties mentioned above will be placed horizontally against a copper coil with a squared useful section with a horizontal gap G_a . In the coil, an alternative current characterized by its density J_E and its frequency F_r circulates. The disk will be placed vertically between two 4340 steel disks of identical shapes and geometries and spaced by a vertical gap G_c . These two disks serve as flux concentrators which have a key role to concentrate the electromagnetic flux in order to reduce the edge effect affecting the piece placed in the middle [20].

Since the geometrical properties of the disk and the inductor coil are invariant by orthogonal symmetry with respect to their symmetry axes, the 3D simulation model can be reduced to a 2D axis-symmetric model, which makes it possible to reduce considerably the calculation and simulation time. Figure 2 illustrates the different geometrical parameters involved in the design of the system.

The machine factors that are involved in the induction heat treatment process are mainly the external current density J_E , the external current frequency F_r , and the heating time T_H .

The study will be done at high frequency, i.e., $F_r = 200$ kHz, and a fast heating time, i.e., $T_H = 0.5$ s. The external current density is to be changed to ensure that the surface temperature of the master disk at the end of heating is greater

Fig. 4 2D model showing nodes to evaluate at the medium and the edge



than the austenitization temperature of the steel 4340, i.e., about 850 °C.

5 Optimization study

The optimization algorithm was implanted using MATLAB in combination with COMSOL multiphasic. It is based on the quasi-Newton method to systematically update the input parameters in order to minimize a predefined objective function. At each iteration, calculation is done using the updated output parameters. The temperature at the edge and the middle of the disk surface is evaluated at each step to verify if it exceeds the minimum austenitization temperature, required to transform the surface structure to austenite. The steps of the finite element optimization method could be summarized in the following flowchart in Fig. 3.

The objective function is an analytic function. The optimization algorithm uses the vector of the parameter $\theta = (\text{radial gap, axial gap})$ to minimize the difference between the middle and the edge profiles' temperature of the part. If this difference is less or equal to the stopping conditions ϵ , then the optimization is complete and a couple of optimal gaps are taken. To summarize, the algorithm's objective is to find the vector θ that minimizes the objective function $F(\theta)$. The objective function is an analytic function defined as:

$$F(\theta) = \sum_{i=1}^n (T_{E_i}(\theta) - T_{M_i}(\theta))^2 \rightarrow \min \tag{1}$$

T_M and T_E are respectively the temperatures at each middle and edge node i after the heating process as illustrated in Fig. 4. θ is the vector of the two parameters, which are the axial gap and the radial gap.

The ranges of the radial gap G_R and the axial gap G_A are very restricted and inspired by the technical and experimental feasibility. The radial gap could vary in the range of 1 to 5 mm, while the axial gap could vary in the range of 0.2 up to 3 mm. The deviation of the axial and radial gaps for each iteration is controlled by the simulation program and varies with a pitch of 0.2 mm for the axial gaps and 0.25 mm for the radial gaps; these values are chosen due to experimental feasibility.

As the study space is confined and well controlled (medium-scale problem), the minima of the objective function will be of the same order, so it is useless to apply global optimization algorithms in this case due to expensive time calculation. The chosen algorithm is that of quasi-Newton [23], which is very useful for non-linear

Table 2 Initial parameters used in optimization process

	Parameter			
	Radial gap	Axial gap	Power	Heating time
Level	3	3	95	0.5
Unit	mm	mm	kW	s

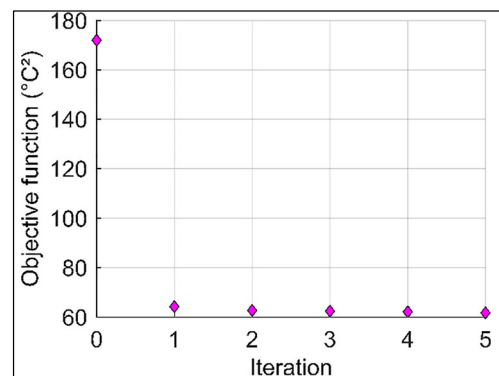


Fig. 5 Evaluation of objective function in each global iteration during optimization process

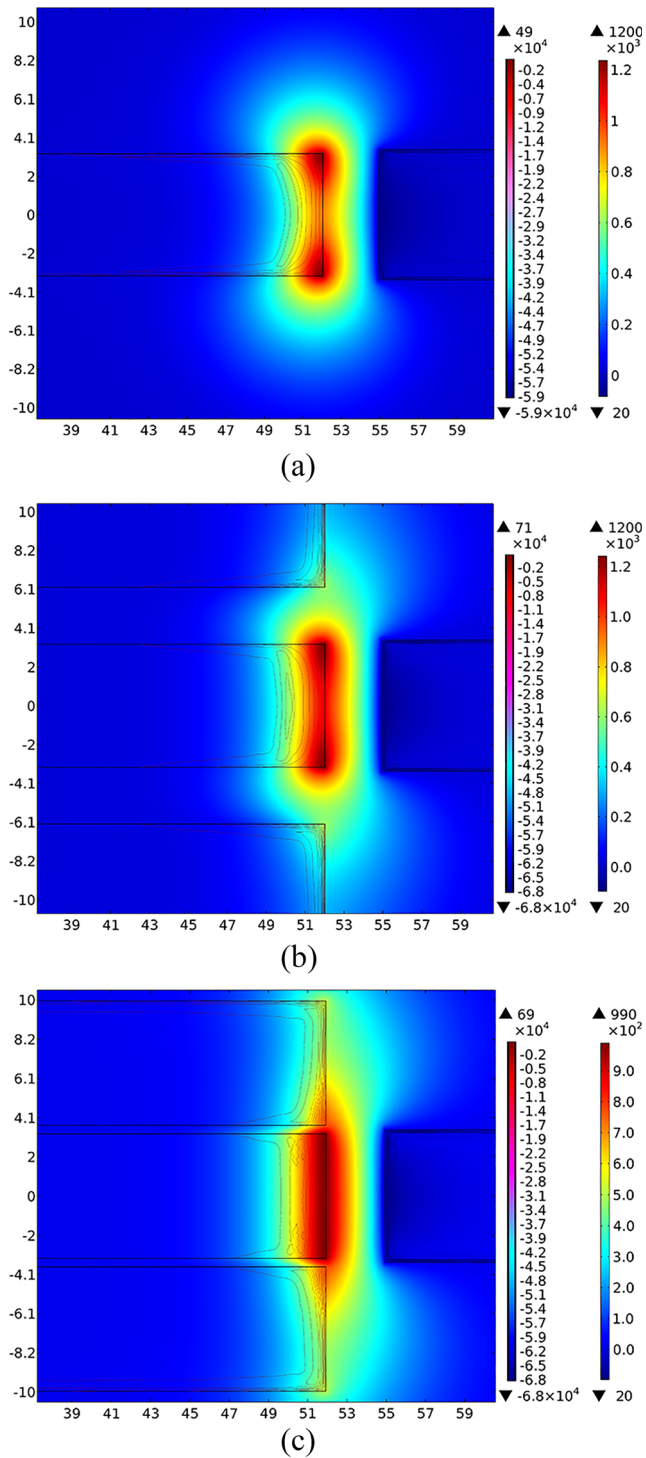


Fig. 6 Induced current (A/m^2) and temperature ($^{\circ}C$) distribution surfaces after the heating process. Induction heating **a** with no flux concentrator, **b** with flux concentrator and initial gap parameters, and **c** with flux concentrator and optimized gap parameters

optimization and black box-type problems. The choice of the quasi-Newton algorithm for optimization is based on two arguments. The first is because the algorithm requires only information about the gradient in each calculation

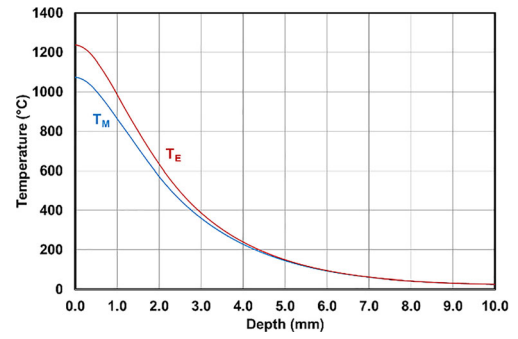


Fig. 7 Temperature profile in the middle and the edges with initial gap parameters

step, and this can be evaluated by discretizing the gradient with the finite difference method at each iteration [24]. The second argument focuses on the ease of calculating the inverse of the Hessian matrix by approximation at each iteration, thus giving speed to the computation and to the optimization process [24].

After obtaining the optimal parameter vector, it suffices to go to the validation step to check the performance of the sized part, with respect to the physical constraints. The result’s accuracy is dependent on the temperature profile’s quality at the surface of the part. The perfect profile is a constant temperature that is higher than the austenitization temperature of the 4340 steel. At the same time, the temperature is gradually decreasing with the workpiece depth. The first property must be introduced in the optimization algorithm as an additional constraint to add to the maximum and minimum bounds on the parameters that must be defined based on physical considerations. Although the chosen structure in this example is simple, the computational load is important, in relation to the computation time either at the level of the finite element modeling steps or at the level of the optimization process; then to obtain a greater precision, it is essential to choose the right parameters of meshes and the criteria of stops for the optimization algorithm. At this point, the choice of initial conditions θ_0 (3 mm, 3 mm) is already done.

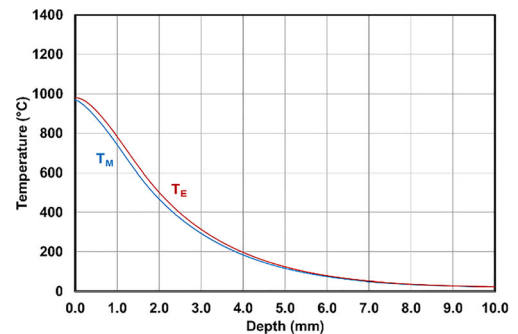
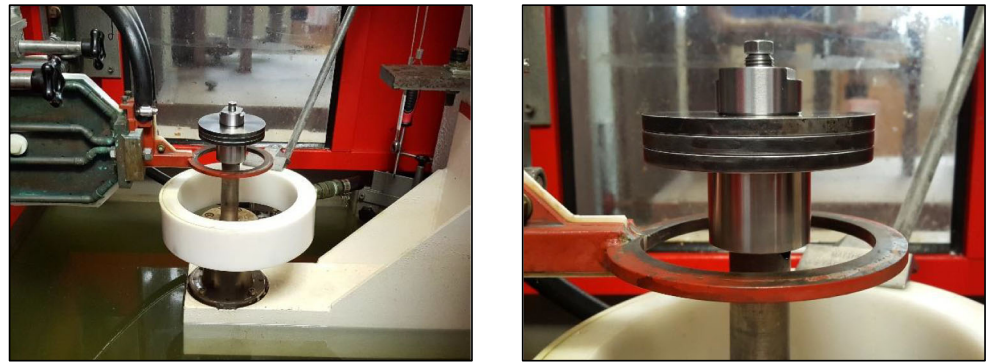


Fig. 8 Temperature profile in the middle and the edges with optimized gap parameters

Fig. 9 Induction machine and operation system



5.1 Numerical simulation

As described above, the study involved the calculation of the inverse Hessian matrix in each iteration, with respect to the constraints defined to guarantee a sufficient heating level at the surface. Simulations started under the following combination are described in Table 2.

As illustrated in Fig. 5, a total of 5 global iterations were performed to reach a local minimum with over 76 numerical calculations that were carried out to evaluate the Hessian matrix with respect to problem constraints. Results lead to an optimized radial gap of 3.1 mm and an optimized axial gap of 0.44 mm. The temperature profile after the heating process under the optimized configuration was analyzed in the middle and the edges of the disk.

Figure 6 illustrates temperature distribution surfaces for the classic induction heating process with no flux concentrators, for the initial non-optimized configuration and for the optimized final configuration with flux concentrators.

In Figs. 7 and 8, the temperature along the radial line is shown to explain the heating penetration depth at the end of the process across the disk. The influence of adjusting the slave flux concentrators and the coil position is observed clearly as the temperature penetrates evenly the core of the disk. High temperatures are maintained in the surface, and the region heated above $AC3 = 780\text{ }^{\circ}\text{C}$ [21] is limited to a depth of about 0.8–0.9 mm from the surface. Martensitic transformation will appear if a fast quenching is achieved by the disk directly after the heating process.

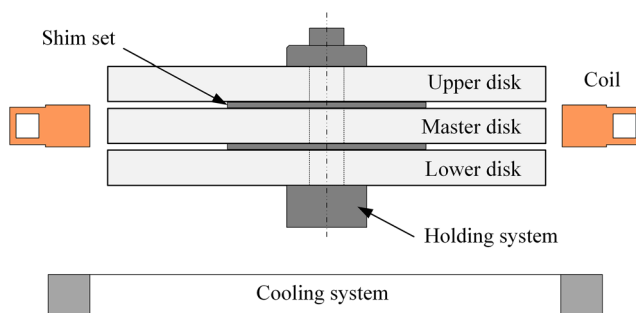


Fig. 10 Experimental setup scheme

Uniform temperature distribution ensures uniform distribution of hard martensite on the surface of the workpiece. Furthermore, the temperature at the surface can be controlled, and higher hardened depths are achievable by increasing the power and the heating time of the process [18]. The effect of flux concentrators and coil position has a light effect on the quantity of energy absorbed by the treated part compared with the power and the heating time. But concentrators and coil position have a much important effect of how this absorbed energy is distributed at the core of the disk.

6 Experimental validation

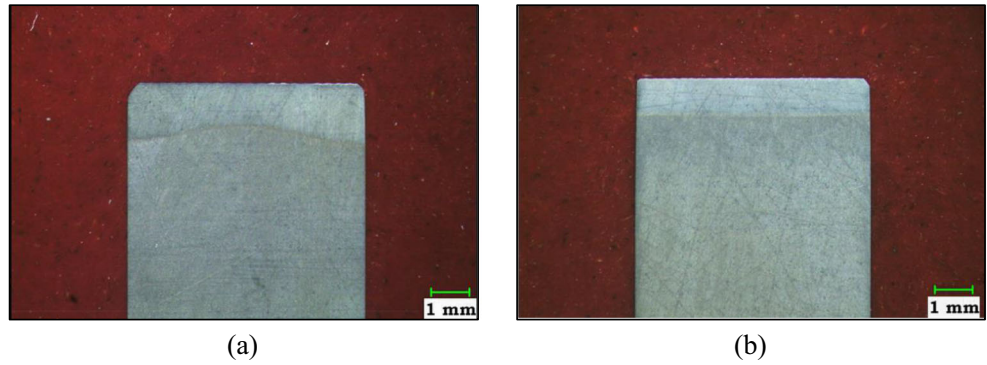
The experimental validation tests were conducted on the induction machine located at the induction heat treatment laboratory at the École de technologie supérieure (Montréal, Canada). This machine is equipped with two medium- and high-frequency power generators. We use the second generator that consists of a thyristor radiofrequency generator (RF), operating at 200 kHz and providing a maximum power of 450 kW.

6.1 Experimental setup

The three disks used for the experimental validation are 4340 steel disks of identical shapes and geometries having an outer diameter of 104.3 mm and a thickness of 6.5 mm. They are placed vertically and spaced by a gap of 0.4 mm as shown in Fig. 9. The master disk and the flux concentrators are mounted together on a prefabricated steel support mounted on the vertical rod of the machine which holds the transverse and rotational movement of the assembly. The spacing between the disk is guaranteed using two 1010 steel shims, used specifically for precision alignment, leveling, and spacing on shafts and machinery. Each shim has a thickness of 0.2 ± 0.05 mm with an outer diameter of 31.75 mm.

The coil is made of copper, and its outer diameter is 140 mm and internal diameter is 110 mm, with a useful section of 49 mm^2 ($7\text{ mm} \times 7\text{ mm}$) with a 2-mm thickness. The

Fig. 11 Hardened profiles revealed after Nital etching **a** with no flux concentrator and **b** with flux concentrators using optimized parameters



cooling of the inductor during heating is ensured with a 38 l/min flow of distilled water. The piece is brought back after the final heating in the shower section where the piece is cooled with jets of a solution with 92% of water and 8% of polymers used in tempering. The shower system is made of PVC and has an outside diameter of 150 mm and internal diameter of 125 mm. The experimental setup is typically the same one used in the simulation model, and it is shown schematically in Fig. 10.

6.2 Metallographic analysis

Figure 11 shows the hardness profiles obtained on the edges of the treated master disk. The brighter and upper regions represent hard martensite transformed after the heating and quenching process while the gray regions are in the form of an un-tempered and non-transformed martensite.

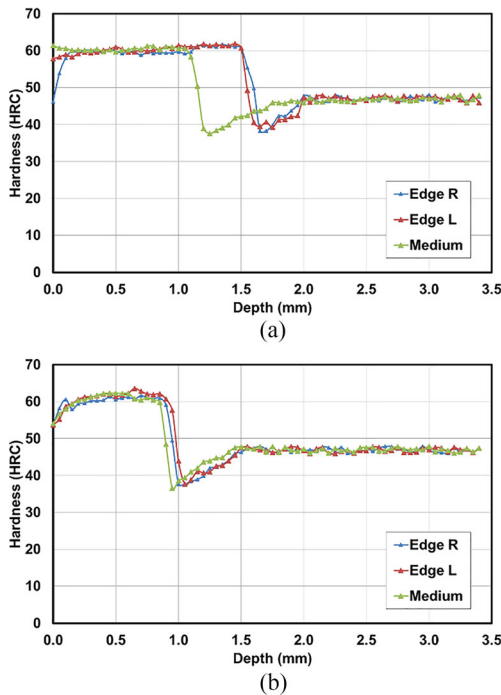


Fig. 12 Hardness profile (a) without flux concentrators and (b) with flux concentrators and optimized parameters

It is clear that the electromagnetic edge effect that causes a non-uniform hardness profile as seen in Fig. 11 has been controlled which leads to a more linear and uniform profile. To quantify this linearity, hardness measurements were made at the three characteristic regions, the middle and both left and right edges. Figure 12 shows the hardness measurements in the predefined regions. Results show that the three curves of hardness have the same appearance. The hardness is maximum at the surface (about 61HRC) and extends to a depth of 0.9 mm which is the hardened or the case depth. The hardness drops drastically from a depth of 1 mm (about 37HRC) and then increases gradually to reach its initial value while approaching the disk core.

7 Discussion

It is well known that the case depth could be extracted directly by simulation from the temperature profile after the heating process [18, 25]. Case depth is related to martensite formation after rapid cooling of austenite. Austenite is only formed in regions where temperature exceeds 800 °C in the case of AISI 4340 [21].

Table 3 and the bar graph illustrated in Fig. 13 represent the measures, the average, and the standard deviation values of

Table 3 Case depth measured for each induction heating method

Case depth (mm)	Classic without flux concentrators	With flux concentrators and no gap optimization	With flux concentrator and gap optimization	With finite element simulation
Left edge	1.5	0.95	0.9	0.95
Middle	1.15	1.1	0.8	0.8
Right edge	1.5	1.15	0.95	0.95
Average	1.383	1.067	0.883	0.900
Standard deviation	0.202	0.104	0.076	0.087

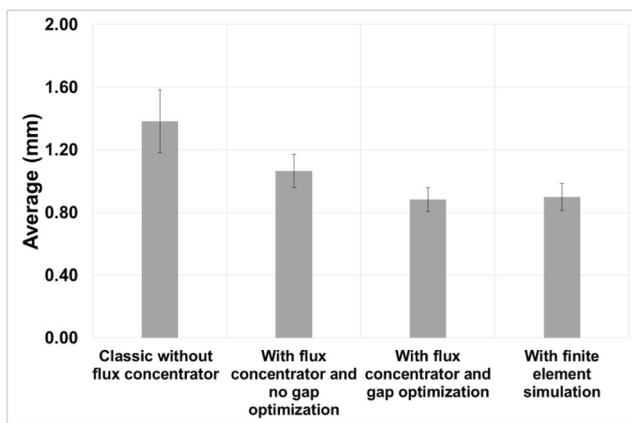


Fig. 13 Bar graph of average and standard deviation of case depth for each induction heating method

the case depth for the left and right edges and middle of the disk for each induction heating process.

The difference between the left edge and the right edge case depth is due to a non-controllable slight dissymmetry of the disk surface toward the coil center during experimental tests. However, the case depth values extracted by simulations present similar results comparatively to case depth values obtained by experiments. Results show a difference on the average of 2% and a difference on the standard deviation of 12% between simulations and experiments. The initial standard deviation of the case depth obtained by a classic induction heating process is about 0.202. Therefore, the presence of flux concentrators has improved the case depth profile by 48.5% with a standard deviation of about 0.104 without gap optimization and improved by 62% with a standard deviation of about 0.076 using gap optimization.

It is evident that the implemented optimization algorithm has succeeded in optimizing the temperature profile to obtain the best case depth profile at the disk surface with respect to the previously imposed constraints. The final temperature at the edge of the part is linear and sufficiently higher than the austenitization temperature.

Despite the fact that the power and heating time during the heating process were kept constant, and the value of the radial gap has been changed to about 0.1 mm, the average final temperature has decreased by 200 °C compared with the initial average, which automatically leads to a decrease in the case depth average of about 0.5 mm compared with the classic induction heating average. This decrease is because the energy supplied by the inductor and consumed by the flux concentrators becomes greater due to the reduction of the axial gap, thus decreasing the energy consumed by the middle part.

To balance the case depth decrease, other process parameters can be adjusted, such as increasing the external current density and the process heating time or adjusting the part or the coil shape. On the other hand, such compensation may lead to a slight increase in the process operating costs, so it

can be said that the optimization is reliable only in relation to the objective initially underlined.

8 Conclusion

This paper has presented an original and comprehensive approach permitting the reduction of the edge effect on the hardness profile of an AISI 4340 disk with flux concentrators and obtaining the best hardness profile using finite element simulation. First, a 2D model has been built using COMSOL by coupling the electromagnetic and thermal fields. Second, an optimization study has been performed to eliminate the edge effect using additional disks acting as flux concentrators. Finally, the simulation model has been validated by a comparative analysis with experiment results. The optimal coil position and gap between the part and flux concentrators permitting the elimination of the edge effect is then founded. It was shown that it is possible to reach the best hardness profile by using the flux concentrator and adjusting the geometrical parameters of the process. Overall, the obtained results show that the simulation is useful also to understand the edge effect and how this phenomenon can be reduced. Consequently, they certainly help induction heating engineers to choose the good parameters for the induction machine and achieve the desired hardness profile. The developed method could be used also to optimize the surface treatment of parts with different shapes like spurs and helical gears.

References

1. Savaria V, et Bridier F, Bocher P (2016) Predicting the effects of material properties gradient and residual stresses on the bending fatigue strength of induction hardened aeronautical gears. *Int J Fatigue* 85:70–84
2. Withers PJ (2007) Residual stress and its role in failure. *Rep Prog Phys* 70:2211–2264
3. Dmytro RC, Krause FN, Friedrich-Wilhelm B, Lorenz G, Bernd B (2012) Investigation of the surface residual stresses in spray cooled induction hardened gearwheels. *Int J Mater Res* 103(1):73–79
4. James MN, Hattingh DG, Asquith D, et Newby M, Doubell P (2016) Applications of residual stress in combatting fatigue and fracture. *Procedia Structural Integrity* 2:11–25
5. Besserer H-B, Dalinger A, Rodman D, Nürnberger F, Hildenbrand P, et Merklein M, Maier HJ (2016) Induction heat treatment of sheet-bulk metal-formed parts assisted by water-air spray cooling. *Steel Res Int* 87:1220–1227
6. Coupard D, Palin-luc T, Bristiel P, Ji V, Dumas C (2008) Residual stresses in surface induction hardening of steels: comparison between experiment and simulation. *Mater Sci Eng A* 487:328–339
7. Deng D (2009) FEM prediction of welding residual stress and distortion in carbon steel considering phase transformation effects. *Mater Des* 30:359–366

8. Ivanov D, Markegård L, Asperheim JI, Kristoffersen H (2013) Simulation of stress and strain for induction-hardening applications. *J Mater Eng Perform* 22:3258–3268
9. Meo M, Vignjevic R (2003) Finite element analysis of residual stress induced by shot peening process. *Adv Eng Softw* 34:569–575
10. Haimbaugh RE (2015) Practical induction heat treating. ASM International, Geauga County
11. Hömberg D, Liu Q, Montalvo-Urquiza J, Nadolski D, Petzold T, Schmidt A, Schulz A (2016) Simulation of multi-frequency-induction-hardening including phase transitions and mechanical effects. *Finite Elem Anal Des* 121:86–100
12. Woodard PR, Chandrasekar S, Yang HTY (1999) Analysis of temperature and microstructure in the quenching of steel cylinders. *Metall Mater Trans B* 30:815–822
13. Li Z, Ferguson BL, Nemkov V, Goldstein R, et Jackowski J, Fett G (2014) Effect of quenching rate on distortion and residual stresses during induction hardening of a full-float truck axle shaft. *J Mater Eng Perform* 23:4170–4180
14. Kristoffersen H, Vomacka P (2001) Influence of process parameters for induction hardening on residual stresses. *Mater Des* 22(8):637–644
15. Nemkov V, Goldstein R, Jackowski J, Ferguson L, Li Z (2013) Stress and distortion evolution during induction case hardening of tube. *J Mater Eng Perform* 22:1826–1832
16. Komotori J, Shimizu M, et Misaka Y, Kawasaki K (2001) Fatigue strength and fracture mechanism of steel modified by super-rapid induction heating and quenching. *Int J Fatigue* 23:225–230
17. Larregain B, Vanderesse N, Bridier F, et Bocher P, Arkinson P (2013) Method for accurate surface temperature measurements during fast induction heating. *J Mater Eng Perform* 22:1907–1913
18. Barka N, et Bocher P, Brousseau J (2013) Sensitivity study of hardness profile of 4340 specimen heated by induction process using axisymmetric modeling. *Int J Adv Manuf Technol* 69:2747–2756
19. Barka N (2017) Study of the machine parameters effects on the case depths of 4340 spur gear heated by induction—2D model. *Int J Adv Manuf Technol* 93:1173–1181
20. Barka N, Chebak A, El Ouafi A, Jahazi M, Menou A (2014) A new approach in optimizing the induction heating process using flux concentrators: application to 4340 steel spur gear. *J Mater Eng Perform* 23:3092–3099
21. Chandler H (1994) Heat treater's guide: practices and procedures for irons and steels. ASM International
22. Senhaji A (2017) Simulation numérique de la chauffe par induction électromagnétique d'un disque en AISI 4340. *École de technologie supérieure*
23. Floudas CCA, Pardalos PM (2006) Encyclopedia of optimization. Springer-Verlag, Berlin
24. Wei Z, et Li G, Qi L (2006) New quasi-Newton methods for unconstrained optimization problems. *Appl Math Comput* 175:1156–1188
25. Barka N, El Ouafi A, et Bocher P, Brousseau J (2013) Explorative study and prediction of overtempering region of disc heated by induction process using 2D axisymmetric model and experimental tests. *Adv Mater Res* 658:259–265

Publisher's note Springer Nature remains neutral with regard to jurisdictional claims in published maps and institutional affiliations.